

# Learning Flexible GEMM Accelerator Configuration and Mapping-space using ML

Ananda Samajdar  
Georgia Tech  
Atlanta, GA

Michael Pellauer  
NVIDIA  
Boston, MA

Tushar Krishna  
Georgia Tech  
Atlanta, GA

anandsamajdar@gatech.edu

mpellauer@nvidia.com

tushar@ece.gatech.edu

**Abstract**—The value of flexibility in Deep Learning accelerators to adapt to diverse layer shapes and sizes is well-understood. Contemporary reconfigurable architectures depend on compilers or other components in the software stack for optimal configuration and mapping search to fully exploit the benefits of flexibility. In this paper we show that the configuration and mapping space of flexible accelerators can be learnt using machine learning by casting it as a classification or recommendation problem. The learnt model can be used to obtain the optimal configuration of the target accelerator in *constant time without search*. We propose ADAPTNET, a recommender system for obtaining optimal configuration and mapping for GEMM workloads running on a RECONFIGURABLE SYSTOLIC ARRAY (RSA). RSA is designed to be configured such that it can operate across a spectrum from a single monolithic array to a distributed collection of smaller arrays of various sizes with flexible aspect ratios. This allows us to simultaneously achieve scalability and high mapping flexibility while preserving operand reuse. ADAPTNET demonstrates 95% test accuracy compared to an exhaustively searched optimal configuration, beating state-of-the-art classification techniques such as SVMs, XGBoost and MLPs. We also present, ADAPTNETX, a specialized core to run ADAPTNET in hardware. Together, RSA and ADAPTNETX enable us to demonstrate a new class of flexible accelerators which are capable of self-configuring in hardware for the given GEMM workload. We present a 32.768 TOPS instance called SAGAR that is capable of providing the same mapping flexibility as a compute equivalent distributed system while achieving 3.5× more power efficiency and 3.2× higher compute density demonstrated via architectural and post-layout simulation.

## I. INTRODUCTION

Custom architecture design enables us to achieve high performance and energy efficiency for a given class of workloads in post Moore’s Law era. Highly specialized architectures however are inflexible to any variation in the nature of workload and thus can easily be rendered obsolete. To mitigate this limitation, there has been an increasing interest in developing flexible architectures which have additional components (interconnects, buffers, and configuration registers) to support changing workload requirements. For popular applications like DNN acceleration, several such flexible architectures have been proposed [10], [11], [12], [22], [37].

In all of the prior works on flexible DNN accelerators, however, the onus of finding and setting the best configuration lies on the software stack, typically using a compiler/mapper [14], [17], [28], [38]. This dependence causes a few deployment challenges: (i) a cost model has to be developed and integrated as an optimizer into the compilation stack to help find optimal

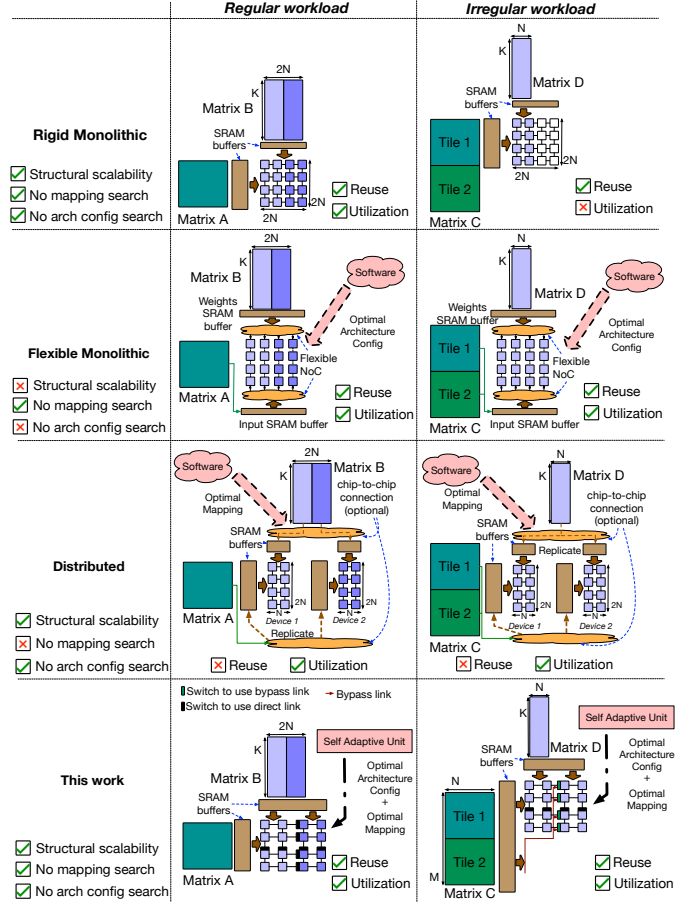


Fig. 1. Comparison of scalability, utilization, and operand reuse in traditional monolithic and distributed accelerators, and the position of the proposed architecture

mappings, without which the flexible design loses utility, (ii) an expensive configuration and mapping search has to be performed at compile-time before scheduling any workload. Usually mapping search in software is performed via exhaustive, heuristic or optimization algorithm-based approaches which take about a few seconds to hours [17], [28], [38], even with sophisticated ML assisted frameworks like autoTVM [4]. (iii) the search-time overhead also eliminates opportunities for deploying such flexible accelerators for domains/applications with soft or hard-real time inference targets.

In this work, we demonstrate that the mapping and con-

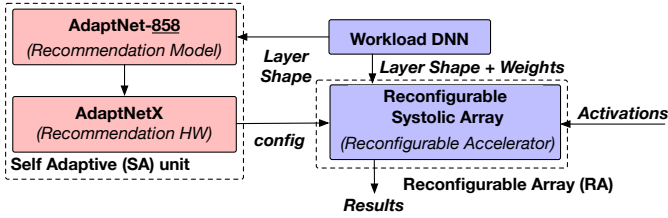


Fig. 2. The constitution and interactions of the self adaptive (SA) and reconfigurable array (RA) components to make up the SARA accelerator called SAGAR in this work.

figuration space of a reconfigurable accelerator can be *learnt* by a machine learning (ML) model, which can then be used to query optimal parameters for any workload at constant time. Dependence on software stack can be eliminated by incorporating this learnt model into the hardware itself and querying it in runtime. We illustrate this via two contributions:

**First**, we design a scalable reconfigurable hardware optimized for GEMM workloads called RECONFIGURABLE SYSTOLIC ARRAY (RSA). RSA is developed upon the intuition that flexible accelerators often need to trade-off utilization, data reuse, and hardware complexity (i.e., scalability). This is illustrated in Figure 1. *Rigid Monolithic* arrays (e.g., TPU’s systolic array [15]), are simple to construct but offer no flexibility leading to high under-utilization for many workloads [30], [33]. *Flexible Monolithic* arrays (e.g., MAERI [22], Eyeriss\_v2 [6], SIGMA [30]) provide flexibility via clever use of interconnects and configuration logic, enabling high utilization for a majority of workloads. However, the increased hardware complexity hinders scaling, and the design requires external software support to exploit the benefits of reconfigurability [14], [17], [28]. Distributed architectures (e.g., Tangram [12], Simba [35]) help address the utilization challenge, since irregular workloads can be tiled on to these smaller arrays. However, this architecture leads to loss in spatial reuse (i.e., direct data-forwarding) that monolithic designs provide, and also requires data replication across the SRAMs of the individual arrays. Data replication leads to a decrease in overall on-chip storage capacity, leading to a loss of temporal reuse due to smaller tiles. Moreover, distributed arrays can exacerbate the mapping search problem [28], [35]. RSA aims to address the shortcomings of all three design strategies. It is a flexible accelerator capable of supporting mappings that can be realized by monolithic as well as distributed arrays by configuring to variable array dimensions and number of sub-arrays (as depicted later in Figure 5(d)), thereby enhancing both utilization and reuse. In practice, RSA closely approximates a flexible monolithic design, with a fraction of area cost.

**Second**, we present a systematic mechanism to cast the architecture configuration as a ML classification problem and discuss considerations for optimal model design, training, and performance of the model at inference. Specifically, we develop a custom ML recommendation system model called ADAPTNET that achieves a recommendation accuracy of 95% on a dataset of 200K GEMM workloads, and on average(GeoMean) 99.93% of the best attainable performance (Oracle). We also design a

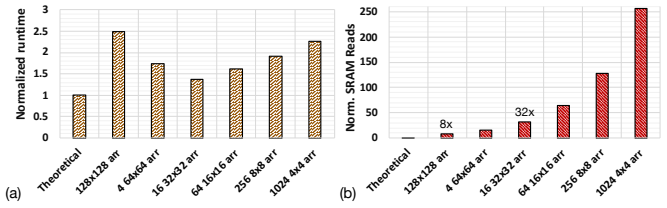


Fig. 3. The trade-off between improved runtime and lost operand reuse in compute equivalent monolithic and distributed systolic array configurations. (a) the theoretical minimum runtime, and the runtime obtained for stall free operation of monolithic and compute equivalent distributed systolic array settings; and (b) the corresponding SRAM reads, normalized to theoretical minimum reads required when multiplying a  $256 \times 64$  matrix with another  $64 \times 256$  matrix.

custom hardware unit to run ADAPTNET called ADAPTNETX. ADAPTNETX enables to get a recommendation response for any query in about 600 cycles which is at least about 6 orders of magnitude faster than software. Furthermore, ADAPTNETX consumes the same hardware real-estate and roughly the same on-chip memory capacity<sup>1</sup> for different arrays, thus proving to be a scalable solution in contrast to approaches like using configuration caches. With ADAPTNETX the configuration lookup using ADAPTNET can be performed at runtime, without involving the software stack.

Together, these two components enable us to develop a new class of accelerators that we call *Self Adaptive Reconfigurable Array (SARA)* (Figure 2). SARA accelerators can self adapt at runtime to optimized configurations for the target workload, without requiring compile-time analysis. We demonstrate an instance of SARA that we name ‘Shape Adaptive GEMM Accelerator (SAGAR<sup>2</sup>)’ as shown in Figure 2 and evaluate its performance across various configurations. We show that SAGAR has  $3.2\times$  higher compute density and  $3.5\times$  improved power efficiency, over equivalent scaled-out systolic array. The extra flexibility costs  $<10\%$  in area and  $50\%$  in power, compared to equivalent scaled-up systolic array. Compared to an area normalized state-of-the-art flexible scalable accelerator [30], SAGAR incorporates  $45\%$  more compute. When comparing compute-equivalent configurations, SAGAR consumes  $43\%$  less power and  $30\%$  less area.

## II. RECONFIGURABLE ARRAY DESIGN

### A. Motivation

To help understand the trade offs involved in choosing a performant configuration, and the associated loss of reuse we perform a simple experiment. We run one GEMM operation, involving operand matrices of sizes  $256 \times 64$  and  $64 \times 256$  on various systolic array configurations. These are, a  $128 \times 128$  monolithic array, and five distributed scale-out configurations viz. 4  $64 \times 64$  arrays, 16  $32 \times 32$  arrays, 64  $16 \times 16$  arrays, 256  $8 \times 8$  arrays, and 1024  $4 \times 4$  arrays. We obtain the runtime and memory accesses for running this workload on all the array configurations using SCALE-Sim [34] (see

<sup>1</sup>The only change in ADAPTNET between various RSA is the weight of the output layer, which is small in comparison to the embedding table which takes most of the on-chip space

<sup>2</sup>means Ocean in Sanskrit, reflecting the shape flexibility of our accelerator.

TABLE I

PREVIOUS ACCELERATOR PROPOSALS CATEGORIZED IN TERMS OF COMPUTATION SUPPORT, AND FLEXIBILITY OF HARDWARE AND MAPPING. ACCELERATORS ARE CATEGORIZED INTO VARIOUS TYPES INTRODUCED IN FIGURE 1 VIZ. RIGID MONOLITHIC (RM), FLEXIBLE MONOLITHIC (FM), AND DISTRIBUTED (DIST)

	Type	Mapping Capability		Dataflow	Flexibility Variable Dimensions	Multi-array Mapping	Self Configurable
		Homogenous	Heterogenous				
Zhang et al. [37]	FM	✓		✓			
Eyeriss [5]	RM	✓					
Alwani et al. [11]	RM		✓				
NeuroCube [18]	Dist		✓			✓	
MAERI [22]	FM	✓	✓		✓		
TPU [15]	RM	✓					
Flexflow [24]	FM	✓		✓			
Tetris [11]	Dist		✓			✓	
Brainwave [10]	Dist		✓			✓	
Simba [35]	Dist		✓			✓	
Tangram [12]	Dist		✓			✓	
Cascades [32]	FM		✓	✓			
Sigma [30]	FM		✓				
Planaria [13]	FM		✓		✓		
SAGAR (This work)		✓	✓	✓	✓	✓	✓

Section V-A). In Figure 3(a) we show the runtime normalized to the theoretical minimum cycles required. Please note that with the chosen matrix dimensions, the systolic arrays in all the configurations are mapped 100% with useful computation. The differences in runtime in various arrays under 100% mapping efficiency is attributed to the array filling and draining at each serialization step (see sec III in [33]). We observe that the configuration with  $32 \times 32$  array is the most performant, beating the monolithic configuration by about  $2 \times$ . In Figure 3(b) we depict the SRAM read accesses performed by all the array configurations, normalized to the theoretical minimum number of reads possible. From this figure we observe that the  $32 \times 32$  configuration performs about  $4 \times$  more memory accesses than the monolithic. The excess memory accesses, which lead to reduced energy efficiency, result from the loss of wire reuse.

From the discussion above we make two observations.

(i) Distributed arrays are more performant than an equivalent monolithic array, even when mapping efficiency is 100% on both. However, the optimal size of each device in a distributed setting is workload dependent. (ii) Monolithic configurations are strictly more energy efficient than distributed arrays, due to loss of spatio-temporal reuse in the latter.

In Table I we inspect a few well known accelerator proposals in terms of scalability and potential to maximize utilization. We notice that simple architectures that are easy to scale in size, under perform on extracting operand reuse. On the other hand, architectures with sufficient flexibility are not scalable. None of the architectures, including the ones with multiple arrays and NoC support, can create variable sized arrays or flexible array dimensions which can help simultaneously achieve high mapping efficiency and data reuse. In the next subsections we develop a flexible design obtained by augmenting a base monolithic systolic array with additional bypass paths along the row and columns. This design enables use to chose between configuration akin to a large single array or a collection of smaller arrays, whenever required.

### B. Compute array

**Traditional MAC units.** In Figure 4(a) we show a traditional systolic array constructed by laying down Multiply-and-

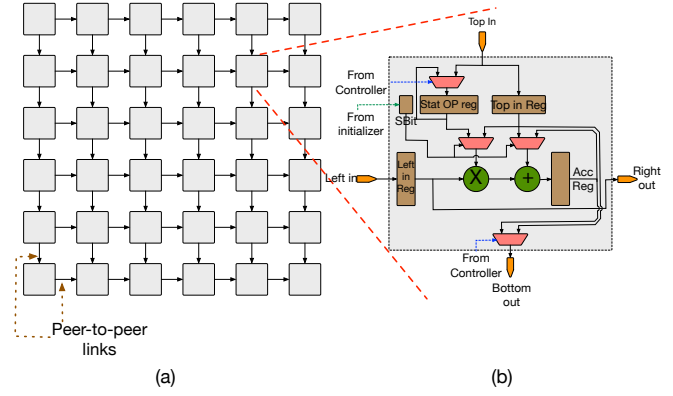


Fig. 4. (a) A systolic array of traditional MAC units, (b) the architecture of a traditional MAC unit

Accumulate (MAC) (Figure 4(b)) units in a 2D grid. Each MAC unit is designed to get an operand from either both (*Left in*, *Top in*) ports or from either of the ports, and perform multiplication and addition operation. In the next cycle the operand data received is sent to its neighbour over the peer-to-peer links. The internal registers, and multiplexers enable the array to work in output stationary (OS), weight stationary (WS), and input stationary (IS) modes of operation [5]. This simple mechanism of data movement results in high wire reuse, but at the same time restricts the mapping of compute only to those operations which require same set of operands to be mapped along a row or a column.

**Systolic Cells.** The mapping flexibility in systolic arrays can be improved by allowing adjacent MAC units to work on different operands. To enable this, the architecture needs to provision for additional links from the SRAM to the MACs. Providing such links to each MAC however is costly in terms of area as well as energy since the spatial reuse over wires is compromised. To simultaneously achieve mapping flexibility and the advantages of spatial reuse in systolic arrays, we propose a design called *systolic-cell*. A *systolic-cell* is a small grid of traditional MAC units augmented with multiplexers at the edges. This enables them to chose the operands from the neighbouring MAC units or a separate set of operands available via bypass links. The MACs within a *systolic-cell* are connected using peer-to-peer links similar to that of a traditional systolic array. Figure 5(a) shows a  $4 \times 4$  *systolic-cell* example. Please note that choice of the size of a *systolic-cell* is implementation dependent. In general, the smaller the cell size, higher the mapping flexibility, which comes at a cost of slightly increased area and power.

**Scale-up and Scale-out using Systolic Cells.** Larger arrays can be created by arranging and connecting the *systolic-cells* as depicted in Figure 5(b) using the peer-to-peer links. At the edge of each *systolic-cell* the muxes can be configured to connect to the bypass links. Please note that dedicated bypass links are allocated to each *systolic-cell* to allow concurrency. Attaining flexible mapping in such a design is a matter of configuring the multiplexers of the *systolic-cells*. Depending on the mapping, an user can chose not to use the bypass paths at all and use the entire array as a single monolithic unit by setting the



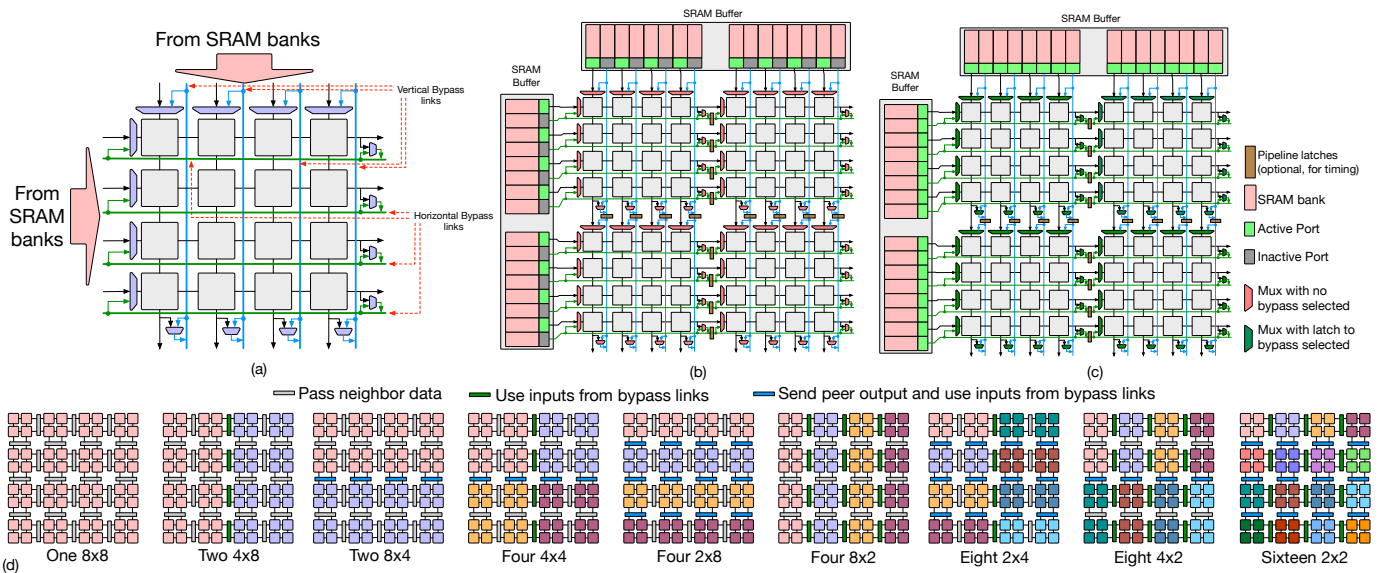


Fig. 5. (a) Construction of a  $4 \times 4$  systolic-cell with bypass muxes and bypass links. (b) A  $8 \times 8$  SMART systolic array operating in scale-up configuration. Each  $4 \times 4$  systolic-cell is connected to its neighbor with the peer-to-peer links as the bypass muxes are turned off. The SRAM ports connected to bypass links are unused. (c) Configuration of bypass muxes to enable the  $8 \times 8$  SMART systolic array to work as a scaled-out distributed collection of systolic arrays. The bypass muxes are turned on to allow systolic-cells to directly connect to the SRAM ports which are all active. (d) Possible monolithic and distributed configurations possible in the reconfigurable Smart-Systolic Array (SSA) using  $2 \times 2$  systolic-cells

multiplexers to accept data only to/from the peer-to-peer links, (this is the case depicted in Figure 5(b)), which is equivalent to a *scaled-up* configuration. On the other hand, the user can set all the multiplexers to accept and deliver data solely to the bypass links, therefore operating as a cluster of arrays, each the size of a systolic-cell. This configuration, depicted in Figure 5(c) is equivalent to a *scaled-out* configuration. Figure 5(d) illustrates some of the possible configurations constructed using a 64 MAC units with  $2 \times 2$  systolic-cells. As can be observed in this figure, not only can the array be configured to work in fully monolithic or fully distributed configurations, but also in any of the configurations in between. By setting the appropriate muxes in either pass-through or bypass modes, sub-arrays larger than systolic-cell size can be constructed (eg.  $4 \times 4$ ,  $8 \times 4$  etc in this example). Each of the sub-arrays have access to the scratchpad memory using the bypass links. Please note that when fully utilized, a larger systolic array improves energy efficiency over a distributed configuration of same number of MAC units by exploiting wire reuse and reducing SRAM reads. The availability of such variety of choices for reconfiguration leads to flexible and efficient mapping, hence improving the utilization and energy efficiency of the design.

### C. Bypass links

Adding a dedicated bypass link from the SRAM bank to each systolic-cell along that row/column is necessary to attain full throughput from the array. Given the nature of the data movements in systolic arrays, we recognize that the vertical links can be used for both second input and the output operands. In Table II, we examine the bandwidth requirements from the bypass links for the three systolic dataflows in a distributed setting, by contrasting it to the requirements of the operands.

These requirements clearly dictate that high bandwidth bypass are necessary. Another addition in our proposed architecture are the switches at the edges of the systolic-cells. However, these switches are simple multiplexers, which are configured statically for a given workload, without the need for any additional logic.

**Scalability via Pipelining.** On-chip wire scalability studies such as SMART [19] have shown that it is possible to traverse a few millimeters (9mm to 11mm) of wire length in 1ns before latching the signal. The authors in SMART achieved this using conventional asynchronous repeaters (a pair of inverters) placed 1mm apart. In RSA, repeated wires offer an opportunity to not only cross a single-systolic cell in a cycle, but in fact bypass multiple systolic cells within a single-cycle. In our reference architecture SAGAR, we perform place-and-route to determine the number of systolic cells per pipeline stage of the bypass links. At 28nm, we find that 8 systolic cells can be bypassed at 1GHz, as we demonstrate later in Section V-B, Figure 13(h). Note that pipelining the bypass links only adds a few cycles of fill time to the RSA, and does not impact the internal timing of the systolic array within each systolic cell (which is itself pipelined at each MAC unit).

### D. Scratch pad memory

The array constructed from systolic-cells is backed by SRAM scratchpad memories, which are constructed as two individual buffers. Each of these buffers is dedicated to one of the operand matrices. Such scratchpad SRAM buffers are common in accelerators, and are designed to reduce the number of off chip accesses and facilitate temporal reuse. Each operand buffer is operated in a double buffered fashion, so that the prefetch latency can be minimized. The system also contains a third buffer which is used to store generated outputs elements.

TABLE II  
BANDWIDTH REQUIREMENTS FOR THE BYPASS LINKS FOR VARIOUS DATAFLOWS, CONTRASTED TO THE REQUIREMENTS OF OPERANDS (NAMES IN PARENTHESIS REFLECTS THE CORRESPONDING OPERANDS IN 2D CONVOLUTIONS)

	Operands		Links		
	Input Mat1 (Activations)	Input Mat2 (Filters)	Outputs	Hor. Bypass	Ver. Bypass
Output Stationary	High	High	Low	High (Inputs)	High (Filters)
Weight Stationary	High	Low	High	High (Inputs)	High (Outputs)
Input Stationary	Low	High	High	High (Filters)	High (Outputs)

```

1 input allLayerParameters | 14
2 input numLayers          | 15
3 for i in (@:numLayers):  | 16
4   layerParameter = allLayerParameters[i] | 17
5   numPartition,   | 18
6   rowPerPartition, colPerPartition, dataflow | 19
7   = recNetInference(layerParameter) | 20
8   setBypassMuxes( numPartition, | 21
9   rowPerPartition, | 22
10  colPerPartition) | 23
11 | 24
12 | 25
13 | 26
14 | 27
15 | 28
16 | 29
17 | 30
18 | 31
19 | 32
20 | 33
21 | 34
22 | 35
23 | 36
24 | 37
25 | 38
26 | 39
27 | 40
28 | 41
29 | 42
30 | 43
31 | 44
32 | 45
33 | 46
34 | 47
35 | 48
36 | 49
37 | 50
38 | 51
39 | 52
40 | 53
41 | 54
42 | 55
43 | 56
44 | 57
45 | 58
46 | 59
47 | 60
48 | 61
49 | 62
50 | 63
51 | 64
52 | 65
53 | 66
54 | 67
55 | 68
56 | 69
57 | 70
58 | 71
59 | 72
60 | 73
61 | 74
62 | 75
63 | 76
64 | 77
65 | 78
66 | 79
67 | 80
68 | 81
69 | 82
70 | 83
71 | 84
72 | 85
73 | 86
74 | 87
75 | 88
76 | 89
77 | 90
78 | 91
79 | 92
80 | 93
81 | 94
82 | 95
83 | 96
84 | 97
85 | 98
86 | 99
87 | 100
88 | 101
89 | 102
90 | 103
91 | 104
92 | 105
93 | 106
94 | 107
95 | 108
96 | 109
97 | 110
98 | 111
99 | 112
100 | 113
101 | 114
102 | 115
103 | 116
104 | 117
105 | 118
106 | 119
107 | 120
108 | 121
109 | 122
110 | 123
111 | 124
112 | 125
113 | 126
114 | 127
115 | 128
116 | 129
117 | 130
118 | 131
119 | 132
120 | 133
121 | 134
122 | 135
123 | 136
124 | 137
125 | 138
126 | 139
127 | 140
128 | 141
129 | 142
130 | 143
131 | 144
132 | 145
133 | 146
134 | 147
135 | 148
136 | 149
137 | 150
138 | 151
139 | 152
140 | 153
141 | 154
142 | 155
143 | 156
144 | 157
145 | 158
146 | 159
147 | 160
148 | 161
149 | 162
150 | 163
151 | 164
152 | 165
153 | 166
154 | 167
155 | 168
156 | 169
157 | 170
158 | 171
159 | 172
160 | 173
161 | 174
162 | 175
163 | 176
164 | 177
165 | 178
166 | 179
167 | 180
168 | 181
169 | 182
170 | 183
171 | 184
172 | 185
173 | 186
174 | 187
175 | 188
176 | 189
177 | 190
178 | 191
179 | 192
180 | 193
181 | 194
182 | 195
183 | 196
184 | 197
185 | 198
186 | 199
187 | 200
188 | 201
189 | 202
190 | 203
191 | 204
192 | 205
193 | 206
194 | 207
195 | 208
196 | 209
197 | 210
198 | 211
199 | 212
200 | 213
201 | 214
202 | 215
203 | 216
204 | 217
205 | 218
206 | 219
207 | 220
208 | 221
209 | 222
210 | 223
211 | 224
212 | 225
213 | 226
214 | 227
215 | 228
216 | 229
217 | 230
218 | 231
219 | 232
220 | 233
221 | 234
222 | 235
223 | 236
224 | 237
225 | 238
226 | 239
227 | 240
228 | 241
229 | 242
230 | 243
231 | 244
232 | 245
233 | 246
234 | 247
235 | 248
236 | 249
237 | 250
238 | 251
239 | 252
240 | 253
241 | 254
242 | 255
243 | 256
244 | 257
245 | 258
246 | 259
247 | 260
248 | 261
249 | 262
250 | 263
251 | 264
252 | 265
253 | 266
254 | 267
255 | 268
256 | 269
257 | 270
258 | 271
259 | 272
260 | 273
261 | 274
262 | 275
263 | 276
264 | 277
265 | 278
266 | 279
267 | 280
268 | 281
269 | 282
270 | 283
271 | 284
272 | 285
273 | 286
274 | 287
275 | 288
276 | 289
277 | 290
278 | 291
279 | 292
280 | 293
281 | 294
282 | 295
283 | 296
284 | 297
285 | 298
286 | 299
287 | 300
288 | 301
289 | 302
290 | 303
291 | 304
292 | 305
293 | 306
294 | 307
295 | 308
296 | 309
297 | 310
298 | 311
299 | 312
300 | 313
301 | 314
302 | 315
303 | 316
304 | 317
305 | 318
306 | 319
307 | 320
308 | 321
309 | 322
310 | 323
311 | 324
312 | 325
313 | 326
314 | 327
315 | 328
316 | 329
317 | 330
318 | 331
319 | 332
320 | 333
321 | 334
322 | 335
323 | 336
324 | 337
325 | 338
326 | 339
327 | 340
328 | 341
329 | 342
330 | 343
331 | 344
332 | 345
333 | 346
334 | 347
335 | 348
336 | 349
337 | 350
338 | 351
339 | 352
340 | 353
341 | 354
342 | 355
343 | 356
344 | 357
345 | 358
346 | 359
347 | 360
348 | 361
349 | 362
350 | 363
351 | 364
352 | 365
353 | 366
354 | 367
355 | 368
356 | 369
357 | 370
358 | 371
359 | 372
360 | 373
361 | 374
362 | 375
363 | 376
364 | 377
365 | 378
366 | 379
367 | 380
368 | 381
369 | 382
370 | 383
371 | 384
372 | 385
373 | 386
374 | 387
375 | 388
376 | 389
377 | 390
378 | 391
379 | 392
380 | 393
381 | 394
382 | 395
383 | 396
384 | 397
385 | 398
386 | 399
387 | 400
388 | 401
389 | 402
390 | 403
391 | 404
392 | 405
393 | 406
394 | 407
395 | 408
396 | 409
397 | 410
398 | 411
399 | 412
400 | 413
401 | 414
402 | 415
403 | 416
404 | 417
405 | 418
406 | 419
407 | 420
408 | 421
409 | 422
410 | 423
411 | 424
412 | 425
413 | 426
414 | 427
415 | 428
416 | 429
417 | 430
418 | 431
419 | 432
420 | 433
421 | 434
422 | 435
423 | 436
424 | 437
425 | 438
426 | 439
427 | 440
428 | 441
429 | 442
430 | 443
431 | 444
432 | 445
433 | 446
434 | 447
435 | 448
436 | 449
437 | 450
438 | 451
439 | 452
440 | 453
441 | 454
442 | 455
443 | 456
444 | 457
445 | 458
446 | 459
447 | 460
448 | 461
449 | 462
450 | 463
451 | 464
452 | 465
453 | 466
454 | 467
455 | 468
456 | 469
457 | 470
458 | 471
459 | 472
460 | 473
461 | 474
462 | 475
463 | 476
464 | 477
465 | 478
466 | 479
467 | 480
468 | 481
469 | 482
470 | 483
471 | 484
472 | 485
473 | 486
474 | 487
475 | 488
476 | 489
477 | 490
478 | 491
479 | 492
480 | 493
481 | 494
482 | 495
483 | 496
484 | 497
485 | 498
486 | 499
487 | 500
488 | 501
489 | 502
490 | 503
491 | 504
492 | 505
493 | 506
494 | 507
495 | 508
496 | 509
497 | 510
498 | 511
499 | 512
500 | 513
501 | 514
502 | 515
503 | 516
504 | 517
505 | 518
506 | 519
507 | 520
508 | 521
509 | 522
510 | 523
511 | 524
512 | 525
513 | 526
514 | 527
515 | 528
516 | 529
517 | 530
518 | 531
519 | 532
520 | 533
521 | 534
522 | 535
523 | 536
524 | 537
525 | 538
526 | 539
527 | 540
528 | 541
529 | 542
530 | 543
531 | 544
532 | 545
533 | 546
534 | 547
535 | 548
536 | 549
537 | 550
538 | 551
539 | 552
540 | 553
541 | 554
542 | 555
543 | 556
544 | 557
545 | 558
546 | 559
547 | 560
548 | 561
549 | 562
550 | 563
551 | 564
552 | 565
553 | 566
554 | 567
555 | 568
556 | 569
557 | 570
558 | 571
559 | 572
560 | 573
561 | 574
562 | 575
563 | 576
564 | 577
565 | 578
566 | 579
567 | 580
568 | 581
569 | 582
570 | 583
571 | 584
572 | 585
573 | 586
574 | 587
575 | 588
576 | 589
577 | 590
578 | 591
579 | 592
580 | 593
581 | 594
582 | 595
583 | 596
584 | 597
585 | 598
586 | 599
587 | 600
588 | 601
589 | 602
590 | 603
591 | 604
592 | 605
593 | 606
594 | 607
595 | 608
596 | 609
597 | 610
598 | 611
599 | 612
600 | 613
601 | 614
602 | 615
603 | 616
604 | 617
605 | 618
606 | 619
607 | 620
608 | 621
609 | 622
610 | 623
611 | 624
612 | 625
613 | 626
614 | 627
615 | 628
616 | 629
617 | 630
618 | 631
619 | 632
620 | 633
621 | 634
622 | 635
623 | 636
624 | 637
625 | 638
626 | 639
627 | 640
628 | 641
629 | 642
630 | 643
631 | 644
632 | 645
633 | 646
634 | 647
635 | 648
636 | 649
637 | 650
638 | 651
639 | 652
640 | 653
641 | 654
642 | 655
643 | 656
644 | 657
645 | 658
646 | 659
647 | 660
648 | 661
649 | 662
650 | 663
651 | 664
652 | 665
653 | 666
654 | 667
655 | 668
656 | 669
657 | 670
658 | 671
659 | 672
660 | 673
661 | 674
662 | 675
663 | 676
664 | 677
665 | 678
666 | 679
667 | 680
668 | 681
669 | 682
670 | 683
671 | 684
672 | 685
673 | 686
674 | 687
675 | 688
676 | 689
677 | 690
678 | 691
679 | 692
680 | 693
681 | 694
682 | 695
683 | 696
684 | 697
685 | 698
686 | 699
687 | 700
688 | 701
689 | 702
690 | 703
691 | 704
692 | 705
693 | 706
694 | 707
695 | 708
696 | 709
697 | 710
698 | 711
699 | 712
700 | 713
701 | 714
702 | 715
703 | 716
704 | 717
705 | 718
706 | 719
707 | 720
708 | 721
709 | 722
710 | 723
711 | 724
712 | 725
713 | 726
714 | 727
715 | 728
716 | 729
717 | 730
718 | 731
719 | 732
720 | 733
721 | 734
722 | 735
723 | 736
724 | 737
725 | 738
726 | 739
727 | 740
728 | 741
729 | 742
730 | 743
731 | 744
732 | 745
733 | 746
734 | 747
735 | 748
736 | 749
737 | 750
738 | 751
739 | 752
740 | 753
741 | 754
742 | 755
743 | 756
744 | 757
745 | 758
746 | 759
747 | 760
748 | 761
749 | 762
750 | 763
751 | 764
752 | 765
753 | 766
754 | 767
755 | 768
756 | 769
757 | 770
758 | 771
759 | 772
760 | 773
761 | 774
762 | 775
763 | 776
764 | 777
765 | 778
766 | 779
767 | 780
768 | 781
769 | 782
770 | 783
771 | 784
772 | 785
773 | 786
774 | 787
775 | 788
776 | 789
777 | 790
778 | 791
779 | 792
780 | 793
781 | 794
782 | 795
783 | 796
784 | 797
785 | 798
786 | 799
787 | 800
788 | 801
789 | 802
790 | 803
791 | 804
792 | 805
793 | 806
794 | 807
795 | 808
796 | 809
797 | 810
798 | 811
799 | 812
800 | 813
801 | 814
802 | 815
803 | 816
804 | 817
805 | 818
806 | 819
807 | 820
808 | 821
809 | 822
810 | 823
811 | 824
812 | 825
813 | 826
814 | 827
815 | 828
816 | 829
817 | 830
818 | 831
819 | 832
820 | 833
821 | 834
822 | 835
823 | 836
824 | 837
825 | 838
826 | 839
827 | 840
828 | 841
829 | 842
830 | 843
831 | 844
832 | 845
833 | 846
834 | 847
835 | 848
836 | 849
837 | 850
838 | 851
839 | 852
840 | 853
841 | 854
842 | 855
843 | 856
844 | 857
845 | 858
846 | 859
847 | 860
848 | 861
849 | 862
850 | 863
851 | 864
852 | 865
853 | 866
854 | 867
855 | 868
856 | 869
857 | 870
858 | 871
859 | 872
860 | 873
861 | 874
862 | 875
863 | 876
864 | 877
865 | 878
866 | 879
867 | 880
868 | 881
869 | 882
870 | 883
871 | 884
872 | 885
873 | 886
874 | 887
875 | 888
876 | 889
877 | 890
878 | 891
879 | 892
880 | 893
881 | 894
882 | 895
883 | 896
884 | 897
885 | 898
886 | 899
887 | 900
888 | 901
889 | 902
890 | 903
891 | 904
892 | 905
893 | 906
894 | 907
895 | 908
896 | 909
897 | 910
898 | 911
899 | 912
900 | 913
901 | 914
902 | 915
903 | 916
904 | 917
905 | 918
906 | 919
907 | 920
908 | 921
909 | 922
910 | 923
911 | 924
912 | 925
913 | 926
914 | 927
915 | 928
916 | 929
917 | 930
918 | 931
919 | 932
920 | 933
921 | 934
922 | 935
923 | 936
924 | 937
925 | 938
926 | 939
927 | 940
928 | 941
929 | 942
930 | 943
931 | 944
932 | 945
933 | 946
934 | 947
935 | 948
936 | 949
937 | 950
938 | 951
939 | 952
940 | 953
941 | 954
942 | 955
943 | 956
944 | 957
945 | 958
946 | 959
947 | 960
948 | 961
949 | 962
950 | 963
951 | 964
952 | 965
953 | 966
954 | 967
955 | 968
956 | 969
957 | 970
958 | 971
959 | 972
960 | 973
961 | 974
962 | 975
963 | 976
964 | 977
965 | 978
966 | 979
967 | 980
968 | 981
969 | 982
970 | 983
971 | 984
972 | 985
973 | 986
974 | 987
975 | 988
976 | 989
977 | 990
978 | 991
979 | 992
980 | 993
981 | 994
982 | 995
983 | 996
984 | 997
985 | 998
986 | 999
987 | 1000
988 | 1001
989 | 1002
990 | 1003
991 | 1004
992 | 1005
993 | 1006
994 | 1007
995 | 1008
996 | 1009
997 | 1010
998 | 1011
999 | 1012
1000 | 1013
1001 | 1014
1002 | 1015
1003 | 1016
1004 | 1017
1005 | 1018
1006 | 1019
1007 | 1020
1008 | 1021
1009 | 1022
1010 | 1023
1011 | 1024
1012 | 1025
1013 | 1026
1014 | 1027
1015 | 1028
1016 | 1029
1017 | 1030
1018 | 1031
1019 | 1032
1020 | 1033
1021 | 1034
1022 | 1035
1023 | 1036
1024 | 1037
1025 | 1038
1026 | 1039
1027 | 1040
1028 | 1041
1029 | 1042
1030 | 1043
1031 | 1044
1032 | 1045
1033 | 1046
1034 | 1047
1035 | 1048
1036 | 1049
1037 | 1050
1038 | 1051
1039 | 1052
1040 | 1053
1041 | 1054
1042 | 1055
1043 | 1056
1044 | 1057
1045 | 1058
1046 | 1059
1047 | 1060
1048 | 1061
1049 | 1062
1050 | 1063
1051 | 1064
1052 | 1065
1053 | 1066
1054 | 1067
1055 | 1068
1056 | 1069
1057 | 1070
1058 | 1071
1059 | 1072
1060 | 1073
1061 | 1074
1062 | 1075
1063 | 1076
1064 | 1077
1065 | 1078
1066 | 1079
1067 | 1080
1068 | 1081
1069 | 1082
1070 | 1083
1071 | 1084
1072 | 1085
1073 | 1086
1074 | 1087
1075 | 1088
1076 | 1089
1077 | 1090
1078 | 1091
1079 | 1092
1080 | 1093
1081 | 1094
1082 | 1095
1083 | 1096
1084 | 1097
1085 | 1098
1086 | 1099
1087 | 1100
1088 | 1101
1089 | 1102
1090 | 1103
1091 | 1104
1092 | 1105
1093 | 1106
1094 | 1107
1095 | 1108
1096 | 1109
1097 | 1110
1098 | 1111
1099 | 1112
1100 | 1113
1101 | 1114
1102 | 1115
1103 | 1116
1104 | 1117
1105 | 1118
1106 | 1119
1107 | 1120
1108 | 1121
1109 | 1122
1110 | 1123
1111 | 1124
1112 | 1125
1113 | 1126
1114 | 1127
1115 | 1128
1116 | 1129
1117 | 1130
1118 | 1131
1119 | 1132
1120 | 1133
1121 | 1134
1122 | 1135
1123 | 1136
1124 | 1137
1125 | 1138
1126 | 1139
1127 | 1140
1128 | 1141
1129 | 1142
1130 | 1143
1131 | 1144
1132 | 1145
1133 | 1146
1134 | 1147
1135 | 1148
1136 | 1149
1137 | 1150
1138 | 1151
1139 | 1152
1140 | 1153
1141 | 1154
1142 | 1155
1143 | 1156
1144 | 1157
1145 | 1158
1146 | 1159
1147 | 1160
1148 | 1161
1149 | 1162
1150 | 1163
1151 | 1164
1152 | 1165
1153 | 1166
1154 | 1167
1155 | 1168
1156 | 1169
1157 | 1170
1158 | 1171
1159 | 1172
1160 | 1173
1161 | 1174
1162 | 1175
1163 | 1176
1164 | 1177
1165 | 1178
1166 | 1179
1167 | 1180
1168 | 1181
1169 | 1182
1170 | 1183
1171 | 1184
1172 | 1185
1173 | 1186
1174 | 1187
1175 | 1188
1176 | 1189
1177 | 1190
1178 | 1191
1179 | 1192
1180 | 1193
1181 | 1194
1182 | 1195
1183 | 1196
1184 | 1197
1185 | 1198
1186 | 1199
1187 | 1200
1188 | 1201
1189 | 1202
1190 | 1203
1191 | 1204
1192 | 1205
1193 | 1206
1194 | 1207
1195 | 1208
1196 | 1209
1197 | 1210
1198 | 1211
1199 | 1212
1200 | 1213
1201 | 1214
1202 | 1215
1203 | 1216
1204 | 1217
1205 | 1218
1206 | 1219
1207 | 1220
1208 | 1221
1209 | 1222
1210 | 1223
1211 | 1224
1212 | 1225
1213 | 1226
1214 | 1227
1215 | 1228
1216 | 1229
1217 | 1230
1218 | 1231
1219 | 1232
1220 | 1233
1221 | 1234
1222 | 1235
1223 | 1236
1224 | 1237
1225 | 1238
1226 | 1239
1227 | 1240
1228 | 1241
1229 | 1242
1230 | 1243
1231 | 1244
1232 | 1245
1233 | 1246
1234 | 1247
1235 | 1248
1236 | 1249
1237 | 1250
1238 | 1251
1239 | 1252
1240 | 1253
1241 | 1254
1242 | 1255
1243 | 1256
1244 | 1257
1245 | 1258
1246 | 1259
1247 | 1260
1248 | 1261
1249 | 1262
1250 | 1263
1251 | 1264
1252 | 1265
1253 | 1266
1254 | 1267
1255 | 1268
1256 | 1269
1257 | 1270
1258 | 1271
1259 | 1272
1260 | 1273
1261 | 1274
1262 | 1275
1263 | 1276
1264 | 1277
1265 | 1278
1266 | 1279
1267 | 1280
1268 | 1281
1269 | 1282
1270 | 1283
1271 | 1284
1272 | 1285
1273 | 1286
1274 | 1287
1275 | 1288
127
```





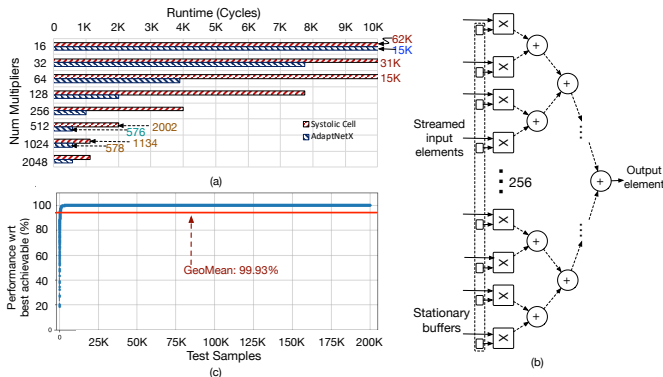


Fig. 9. (a) Cycles needed to run ADAPTNET-858 on an array of *systolic-cells* and on the custom hardware unit (ADAPTNETX) as a function of number of multipliers. (b) Architecture of the custom 1-D unit hardware for ADAPTNETX (c) Relative performance of the configurations predicted by ADAPTNET-858 for SAGAR for  $2 \times 10^5$  test samples when compared to the runtime of best possible configurations

therefore we call the corresponding network ADAPTNET-858.

### C. Alternatives to ADAPTNET

Memoization, in form of caching is one alternative to ADAPTNET to attain constant time configuration lookup. However, caching only works for a limited number of previously computed workloads. For any workload which does not hit in the cache, search has to be performed at runtime. The large configuration space of RSA as depicted in Figure 7(a) makes it a non scalable solution. On the other hand, ADAPTNET, owing to learned parameters, can generalize configuration recommendation to any query having workload dimensions generated from the distribution of its training dataset.

## IV. SELF ADAPTIVE RECONFIGURABLE ARRAYS

By coupling ADAPTNET with a reconfigurable array, we can create a self adaptive system which can be conceptually viewed as a combination of two units, a Self Adaptive unit (SA), and a Reconfigurable Array (RA) unit as shown in Figure 2. The SA unit encompasses the software and hardware components which recommend the optimal configurations. The RA unit is the hardware unit capable of flexibly configuring to the recommended configurations and hence run the workloads. It is worth pointing out that this design class is not specific to a reconfigurable core for running GEMM workloads. Instead any Coarse Grained Reconfigurable Array (CGRA) unit, configurable at runtime, can be augmented with a suitable SA, to ensure optimal performance. We believe this results in a new class of designs, which we name Self Adaptive Reconfigurable Array (SARA).

### A. Hardware to run ADAPTNET

In the context of our use case, an intuitive option is to allocate a few *systolic-cells* from the main array to run ADAPTNET. However, this choice will lead to either fewer MAC units left for the actual workloads, or to allocate additional *systolic-cells* for ADAPTNET leading to an additional overhead. An alternative to adding more *systolic-cells* will be to add a custom hardware

dedicated for running ADAPTNET. We explore both the *systolic-cell* and custom hardware options below for ADAPTNET-858.

**ADAPTNET Runtime on *systolic-cells*.** Figure 9(a) shows the cycles required for a single inference of the ADAPTNET as a function of multipliers used in  $4 \times 4$  *systolic-cell* based array. Understandably, the runtime decreases proportional to the increase in number of multipliers as we increase the number of *systolic-cells*, achieving the best runtime of 1134 cycles when using 1024 multipliers or 64 cells. When both the workloads and the recommendation engine is run on a same array; for a TPU equivalent machine with  $2^{14}$  MAC units, about 6.25% of the array needs to be allocated for running the ADAPTNET. Another choice could be allocating more hardware resources in terms of extra 64 *systolic-cells* dedicated to run the recommender network. However, given that ADAPTNET has exclusively dense layers processing the embedding lookups, a *systolic* execution turns out to be sub-optimal.

**ADAPTNET Runtime on ADAPTNETX.** We found a custom design tuned for ADAPTNET layer parameters to be more efficient. For efficient execution of the dense layers, we chose a 1-D multiplier unit with a binary tree based reduction as shown in Figure 9(b). We found Input stationary (IS) dataflow to be the most performant for our use case. In this mapping the elements of the input vector is buffered near the multipliers, while elements of the weight matrix are streamed through to generate one output element/partial sum, with a sustained throughput of 1 element per cycle. Throughput can be further increased by adding more such 1-D units. We name the custom core with one or more such 1-D units as ADAPTNETX. In Figure 9(a) we depict the variation of runtime of ADAPTNET inference on ADAPTNETX with two 1-D units as a function of multipliers. We find the 512 multipliers result in best runtime of 576 cycles, when running ADAPTNET for  $2^{14}$  MAC unit *systolic-cell* design. We also examine the cost of misprediction of ADAPTNET in Figure 9(c), where we plot the runtime of the predicted configurations from ADAPTNET-858 normalized to best possible runtime. We see that most mispredictions are benign and only a few misprediction lead to catastrophic performance losses, leading to a geometric mean of 99.93% of the best possible performance.

### B. SAGAR Accelerator

SAGAR is constructed by augmenting the  $2^{14}$  MAC RSA unit, laid out as  $32 \times 32$  grid of *systolic-cells*, with ADAPTNETX running ADAPTNET-858 (see Figure 10). We chose this configuration as it has the same compute as the TPU v2, and the  $4 \times 4$  *systolic-cell* size works the best for our workloads (see Section V-A). Since each row and column in this configuration has 31 bypass links and one link to MAC, each buffer is constructed as a collection of 1024 1KB banks.

**Real-time Reconfiguration.** The ADAPTNETX uses an additional SRAM bank of 512KB to store the embedding table and the weight matrices for ADAPTNET-858. Each configuration corresponds to a 3968 bit vector which sets the bypass muxes, once the layer is ready to be mapped.

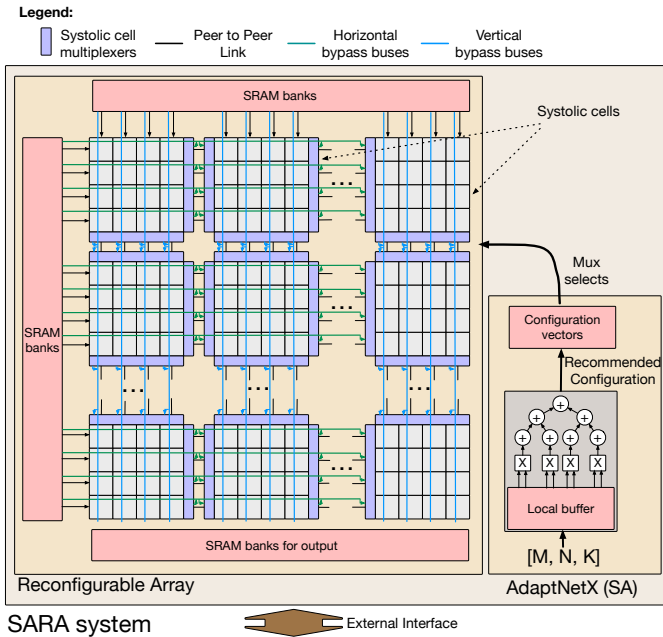


Fig. 10. Schematic of *SAGAR*, an instance of a SARA accelerator.

TABLE III  
 TABLE DEPICTING THE ARCHITECTURAL CONFIGURATION OF DISTRIBUTED SYSTOLIC ARRAY BASED SYSTEMS, MONOLITHIC SYSTOLIC ARRAY BASELINE, AND *SAGAR*

Name	Num Units	MAC/unit	Banks per SRAM buffer	Capacity per SRAM bank
Dist. 4x4 units (Baseline)	1024	16	4	256 B
Dist. 8x8 units	256	64	8	512 B
Dist. 16x16 units	64	256	16	1 KB
Dist. 32x32 units	16	1024	32	2 KB
Dist. 64x64 units	4	4096	64	4 KB
Monolithic 128x128 (Baseline)	1	16384	128	8 KB
<b><i>SAGAR</i></b>	<b>1</b>	<b>16384</b>	<b>1024</b>	<b>1 KB</b>

## V. EVALUATIONS

We evaluate *SAGAR* in two settings. To capture the merits of the architecture, we present results obtained from simulation. While the implementation aspects are captured by reporting PPA number obtained from Place-and-Route (PnR).

### A. Architectural evaluations

**Methodology.** For our architecture level studies we chose to use SCALE-Sim [34]. SCALE-Sim is a cycle accurate simulator for systolic array, which generates per cycle data accesses to and from various memories. This enables us to estimate and compare performance, energy consumption, power etc. of systolic array based components to a certain degree of accuracy. We created in-house scripts to generate SCALE-sim input files to perform the workload partitioning for the configurations recommended by ADAPTNET-858.

**Workloads.** For our evaluations we choose FasterRCNN [31], DeepSpeech2 [2], and AlphaGoZero [36], as our workloads as a representative of convolution neural networks,

TABLE IV  
 DIMENSIONS FOR THE SYNTHETIC GEMM WORKLOADS

	G1	G2	G3	G4	G5	G6	G7	G8	G9	G10
M	128	256	512	1024	2048	128	256	512	1024	2048
K	128	256	512	1024	2048	64	64	64	64	64
N	128	256	512	1024	2048	64	64	64	64	64
	G11	G12	G13	G14	G15	G16	G17	G18	G19	G20
M	64	64	64	64	64	64	64	64	64	64
K	64	64	64	64	64	128	256	512	1024	2048
N	128	256	512	1024	2048	64	64	64	64	64

language modelling network, and DNNs for reinforcement learning respectively. Figure 11(f-g) shows our sensitivity analysis using a few other well known networks.

**Baselines.** We chose a  $128 \times 128$  monolithic systolic array and distributed array of  $1024 \ 4 \times 4$  arrays as our baselines as depicted in Table III. Both the arrays have same number of MAC units as TPUv2. Each array in distributed configuration resembles the tensor cores in Nvidia GPUs. Both that baselines have the same total SRAM memory capacity of 3MB divided into buffers for staging two operand and one output matrix.

**Performance Analysis.** We model both of the baseline systems and *SAGAR* in SCALE-Sim and compare the performance for our workloads. In Figure 11(a) we depict the cycles taken to run all the layers in AlphaGoZero, DeepSpeech2, and the first 10 layers of FasterRCNN networks. Among the baselines, the distributed configuration mostly results in faster runtime owing to higher mapping flexibility. However *SAGAR*, owing to reconfigurability is capable of matching the better baseline configuration. Naturally, this flexibility leads to lower aggregated runtime for *SAGAR* than either of the baselines. We see this trend generalizing in Figure 11(f) as well.

**systolic-cell Design Space Exploration.** *SAGAR* is also capable of realizing configurations which are out of scope of either of baselines. This allows *SAGAR* to achieve higher performance than both the baselines on certain layers. For example, consider the synthetic GEMM operands depicted in Table IV. Figure 12(a) depicts the histogram of the best configuration for these layers obtained from simulation. The layers favouring  $8 \times 8$  or  $32 \times 32$  configurations constitute about 40% of the set. Neither of these configurations can be realized a fixed array configuration like the baselines. In Figure 12(b,c,d) we show the histogram of a similar experiment conducted on our DNN workloads. For these specific workloads, the  $4 \times 4$  configuration works the best for majority of the layers. This observation also explains our findings in Figure 11(a) on why *SAGAR*'s performance is identical to the  $4 \times 4$  baseline. Nevertheless, for layers which favor configurations like  $8 \times 8$ ,  $32 \times 32$  etc. *SAGAR* will lead to lower runtime than both the baselines. This is depicted by Figure 11(c), where we see that *SAGAR* achieves about  $> 10 \times$  speedup over monolithic when distributed configurations are preferred. While in cases where monolithic is preferred it runs faster than both the baselines.

**SRAM reads and Energy efficiency.** In general, due to the loss of reuse, distributed configurations with smaller array sizes have more SRAM reads resulting in lower energy efficiency. We observe this trend in action in Figure 11(b) where we depict the number of SRAM reads performed for layers when running our



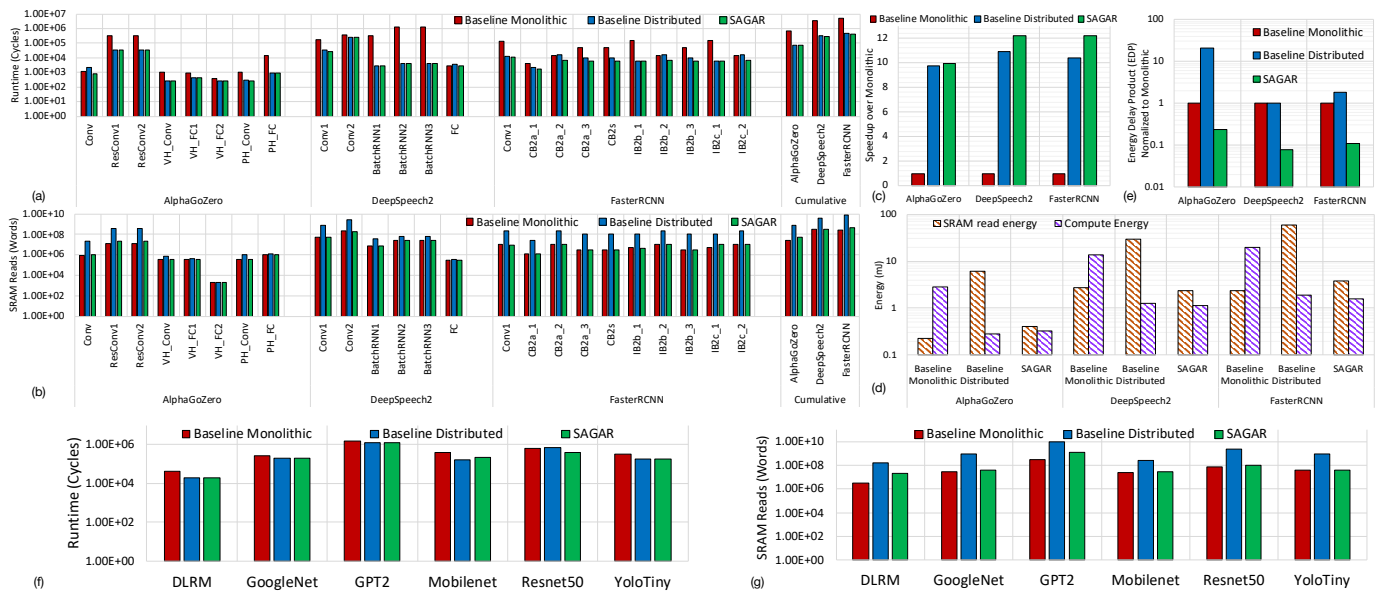


Fig. 11. (a) Simulated runtimes for monolithic  $128 \times 128$  baseline, distributed  $1024 \times 4 \times 4$  baseline, and *SAGAR* for layers in AlphaGoZero, DeepSpeech2, and first 10 layers of FasterRCNN (b) SRAM reads for the same workloads for *SAGAR* and baseline configurations (c) Speedup of *SAGAR* and distributed baseline as compared to the monolithic baseline (d) Energy consumption breakdown for our workloads in *SAGAR* and baselines (e) Energy delay product (EDP) of *SAGAR* and baselines, normalized to EDP for monolithic baseline (f-g) Sensitivity analysis on various networks for runtime and SRAM reads

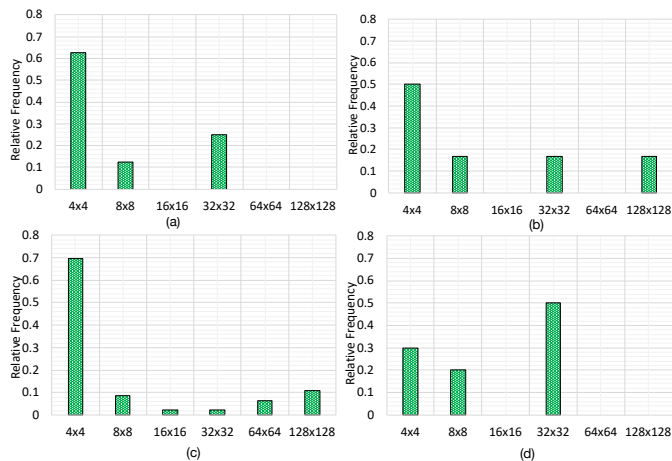


Fig. 12. Distribution of favorable array sizes for a 16384 MAC distributed system which attain the lowest runtime when run for each layer in (a) synthetic GEMM workloads (b) AlphaGoZero, (c) DeepSpeech2, and (d) FasterRCNN.

workloads on the two baselines and on *SAGAR*. The distributed  $4 \times 4$  system has much higher number of reads as compared to *SAGAR* and the monolithic baseline. In *SAGAR* this efficiency loss in reuse is mitigated by using bypassing links. As shown in Figure 11(b), across all layers in our workloads, *SAGAR* incurs SRAM reads close to that in the monolithic baseline. In the case of DeepSpeech2, *SAGAR*, owing to efficient mapping, incurs reads even fewer than that of the monolithic baseline. Similar trends are also reflected in other networks as well (Figure 11(g)). To further quantify the efficiency of *SAGAR*, we estimated the energy spent by the three configurations on the workloads by taking into account the cycle counts and the SRAM reads and scaling the counts by typical energy consumed per operation

computed from RTL PnR flows. For all the workloads, the wire energies calculated using 100 fJ/bit-mm at 14nm [7], come to be about 0.1% (maximum being 0.11% or 0.8uJ in AlphaGoZero), which is negligible. In Figure 11(d) we plot the energy consumed for the three workloads on the baselines and *SAGAR*. We observe that for workloads amenable to monolithic array (ie. FasterRCNN and DeepSpeech2), *SAGAR*'s energy consumption is almost identical to the monolithic baseline. The distributed baseline on the other hand consumes an order of magnitude higher energy for all the three workloads, while supporting the same mapping configurations as *SAGAR*. The difference in energies are a direct consequence of utilization. Since fine grained power or clock gating is impractical, the arrays with poor utilization consume same amount of power as the arrays with better utilization. However, these arrays take longer to complete resulting in higher energy consumption. For AlphaGoZero, which favours a distributed configuration, *SAGAR* consumes about 20% of the energy consumed by the monolithic baseline, while almost one order of magnitude lower than that of the distributed baseline. Figure 11(d) also shows that *SAGAR*'s energy consumption for SRAM is close to that consumed by the monolithic array for all the three workloads. The computation energy consumption in *SAGAR* equivalent to the better of the two baselines. The combined effect of improved latency and reuse is perhaps better represented by the energy-delay product (EDP) depicted by Figure 11(e). In this figure we plot the EDP for *SAGAR* and the two baselines normalized to the values corresponding to the monolithic configuration. We observe that *SAGAR* results in about 92% to 80% less EDP compared to the monolithic baseline. This further demonstrates the efficiency of our proposed architecture, resulting from

preserving reuse while simultaneously decreasing latency due to improved mapping.

### B. Implementation evaluations

**Methodology.** We implemented SAGAR in RTL as a  $32 \times 32$  array of  $4 \times 4$  *systolic-cells* and ran ASIC flow till Place-and-Route (PnR) to obtain area and power. We used 28nm library for implementing the logic. We also implemented the SRAM buffers as a collection of 1024 1KB cells with the SAED32 education library from Synopsis, to quantify the power and area overheads, and then scaled down to 28nm equivalent by using Dennard’s scaling [9]. Figure 13(a) depicts the post PnR floorplan of SAGAR’s compute logic. Figure 13(b) lists the array configuration, area, and power consumption reported after PnR by synthesizing the RSA and memory at a operating frequency of 1 GHz. At 32.768 TOPs (with 1 MAC being two operation) at 1 GHz SAGAR takes 81.90  $mm^2$  of real estate while consuming 13.01 W of power. ADAPTNEX consumes 8.65% of area and 1.36% of power.

**Baselines.** We implement the baseline monolithic  $128 \times 128$  systolic array and distributed  $4 \times 4$  array in RTL. The distributed array is implemented using 1024 identical  $4 \times 4$  traditional systolic arrays connected together by a mesh interconnect. We used the OpenSMART [21] tool to generate and synthesize the mesh topologies for these systems.

The total memory capacity of both the monolithic and the distributed configurations are kept the same at 3MB. As discussed in Section V-A the monolithic array has two input operand buffer of 1MB each and an output buffer also with the 1MB capacity. In our implementation, we opted for one bank per row or column of the array. This choice ensures that each incoming link to the array will have full bandwidth from SRAM provided that bank conflicts are negligible. Therefore each buffer in the monolithic baseline is constructed using 128, 8KB banks. For the distributed configuration, for each  $4 \times 4$  array we end up with 1MB for each operand buffer. Using the same design approach as above, we end up with each buffer being constructed using 4 banks of 256 words each. In Table III we extend the same design principle for designing the memory for various other cell sizes and for SAGAR. In SAGAR, in addition to the links going directly from the SRAM to the edge MAC units of the array, we have to consider the bypass links as well. To get full bandwidth on these links we need to consider additional buffers. Extending the design described in Figure 5, each row and column of SAGAR has 31 bypass links and one link to the first MAC unit, we need 32 banks per row/column. Therefore each SRAM buffer is constructed with 1024, 1KB banks.

**Area Analysis.** In Figure 13(c) we depict the break down of area overheads for SRAM buffers, mesh NoC, and the compute array for various distributed configurations, the monolithic array, SAGAR and SIGMA [30]. We observe that the monolithic configuration is the most efficient in terms of area, where it is about  $5 \times$  more compact than the distributed  $4 \times 4$  array configuration. The breakdown suggests that the bloating in the distributed  $4 \times 4$  configuration is caused predominantly by the Mesh NoC (contributing to 40.5%), followed by the

SRAM buffers. SAGAR on the other hand takes about 8% more area than the monolithic array, while consuming about  $3.2 \times$  lower area than the distributed  $4 \times 4$  configuration. Considering both SAGAR and the distributed configuration provides same mapping flexibility, the proposed design is strictly more efficient.

**Power Consumption.** In Figure 13(d) we depict the post PnR power consumption for various array configuration. The Mesh NoC stands out as the major contributor, which naturally makes the  $4 \times 4$  distributed configuration about  $5.3 \times$  more expensive than the monolithic configuration, with the NoC contributing to about 78% of the power. Considering the power of the compute array alone, all the systolic-array based configurations appear to consume similar power. We also depict the trend in power consumed by SRAM banks across various systolic-array based configurations in Figure 13(f). Similar to the trends observed in area breakdown, the counter balancing affects of increasing the bank sizes and lowering of number of banks lead to similar powers across various distributed and monolithic configurations.

RSA however consumes about 50% more power than the monolithic configuration, owing to the bypass links. However this extra cost results in achieving the same mapping flexibility of the  $4 \times 4$  distributed configuration, which is about  $3.5 \times$  more expensive.

**Scalability Analysis.** (i) Figure 13(g) we show the overhead of using smaller *systolic-cell* sizes in terms of area and power normalized to monolithic configuration. For specific use cases with relaxed requirements for flexibility larger sized *systolic-cells* can be used to improve the implementation costs. (ii) Figure 13(h) we depict the max frequency that can be met as a function of number of  $4 \times 4$  *systolic-cells* that can be bypassed at 28 nm. Since we target 1GHz, we need to pipeline the bypass paths by inserting flops after 8 *systolic-cells* as we discuss in Section II-C.

### C. Comparison with SIGMA

**Implementation Comparison.** We compare the area of SAGAR with the published area and power numbers of a state-of-the-art flexible accelerator SIGMA [30]. SIGMA allocates a significant portion of area for NoC, which together with SRAM comprise about 80% of the total area Figure 13(c). In SAGAR, simple bypass links are used to achieve the flexibility, which saves about 30% of the area in comparison. From Figure 13(d), we observe that NoC is SIGMA consumes about  $1.8 \times$  more power than SAGAR, with NoC consuming 45% of total power.

**Performance Comparisons.** We use the analytical model used in the original paper <sup>3</sup> to estimate performance of SIGMA [30], which accounts for the time taken to stream, compute, and add partial sums as per the functionality described in their paper. In Figure 14(a) we plot the simulated runtimes for SAGAR, monolithic baseline, and SIGMA with equal number of MAC units (denoted as SIGMA\_C) for our representative workloads and the ten layers reported in the SIGMA paper. SIGMA\_C outperforms SAGAR in all workloads. This is due

<sup>3</sup>We thank the authors of SIGMA for their gracious support

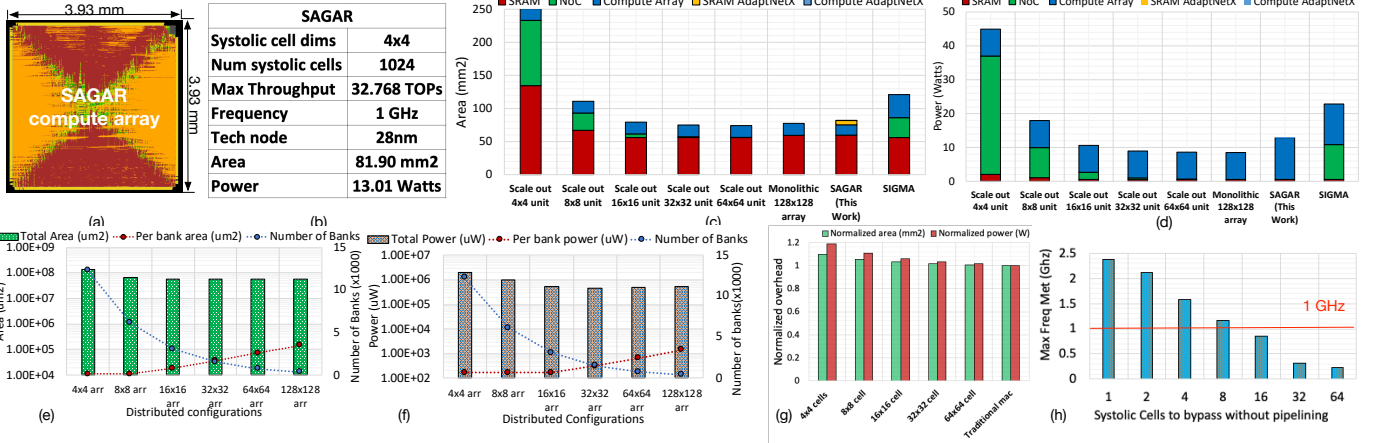


Fig. 13. Design-space exploration and final architecture of *SAGAR*. (a) The post PnR floor-plan diagram of *SAGAR*'s compute array, (b) A table detailing architecture configuration of *SAGAR*, the implementation parameters, and post PnR area and power of *SAGAR*. (c) The comparison and breakdown of post synthesis area for distributed systolic array based designs, the monolithic systolic baseline, *SAGAR*, and *SIGMA* (d) The corresponding breakdown for power consumed by various components in distributed systolic array based designs, the monolithic systolic baseline, *SAGAR*, and *SIGMA* (e) The variation of total area footprint of SRAM banks in various distributed systolic array and monolithic configuration juxtaposed with the variation in bank sizes and the number of banks required, (f) A similar variation in the power consumption by the SRAM banks in distributed systolic array and monolithic configurations, and (g) the the area and power of a  $128 \times 128$  array when constructed using different sized of “systolic-cells” normalized to the area and power of an array constructed with traditional MAC units. (h) The maximum attainable frequency vs the number of  $4 \times 4$  systolic-cells to bypass at 28nm.

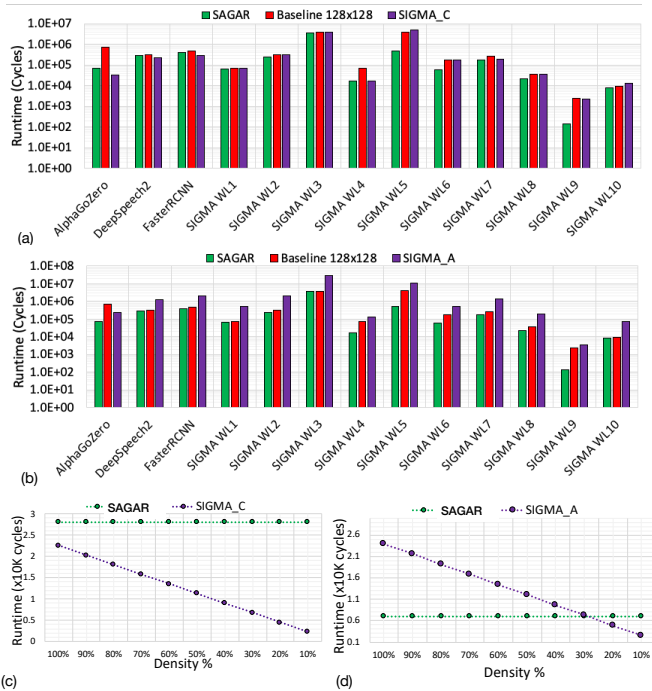


Fig. 14. Runtimes obtained for (a) running dense workloads for monolithic baseline, *SAGAR*, and *compute normalized* configuration of Sigma (*SIGMA\_C*), (b) dense workloads for monolithic baseline, *SAGAR*, and *area normalized* configuration of Sigma (*SIGMA\_A*); and (c) *SAGAR* and *SIGMA\_C* configuration by increasing levels of sparsity (decreasing density) in DeepSpeech2, (d) *SAGAR* and *SIGMA\_A* configuration by varying levels of sparsity in AlphaGoZero

to the fact that the operands are directly streamed to the multiplier over the heavy Benes network, whereas in *SAGAR*, the store-and-forward operation takes up some cycles. The gap

in performance further widens with the increase in sparsity as shown in Figure 14(c).

As *SIGMA* implementation takes more area than *SAGAR*, we also compare against the area normalized configuration (2734 MACs) of *SIGMA* (denoted as *SIGMA\_A* in Figure 14) for fairness. In this case, *SIGMA\_A* consumes about an order of magnitude more number of cycles for each workload as compared to compute normalized configuration, therefore rendering *SAGAR* as the best performer (Figure 14(b)). Even when considering workloads with sparse operands, *SIGMA\_A* is able to surpass *SAGAR* only at operand sparsity values above 70% (see Figure 14(d)).

## VI. RELATED WORKS

**Flexible DNN Accelerator.** Table I depicts the standing of various such accelerators in term of native operation supported, mapping capability and flexibility. Designs like [18], [24], [37], [13], [10], [30], [22], [32], [1], [12], [37] have limited flexibility in either reconfigurability or dataflow. The RECONFIGURABLE SYSTOLIC ARRAY enables both mapping flexibility and reconfigurability.

**Dataflow and Accelerator Design Space Search.** Contemporary tools [33], [20], [11], [28], [8] etc enable DSE by fast cost estimation or heuristics. SARA systems like *SAGAR* on the other hand obtain optimized configuration at runtime in one-shot using ADAPTNET.

**ML assisted system configuration.** Recent work [16], [17], [27] show using GAs for efficient search. RL and recommendation has been used for chip PnR [23], [25]. AutoTVM [4] use ML models for cost prediction to improve compilation time. It is worth noting that these approaches mostly enhance search for the optimal configuration, while ADAPTNET replaces search.



## VII. CONCLUSIONS

This work shows that the mapping and configuration space of reconfigurable accelerator can be learnt using ML. We demonstrate this by developing a recommendation model called ADAPNET which learns and predicts the optimal configurations for RSA with high accuracy. RSA is a flexible, scalable GEMM accelerator constructed using *systolic-cells* and pipelined bypass paths.

## REFERENCES

- [1] M. Alwani, H. Chen, M. Ferdman, and P. Milder, "Fused-layer cnn accelerators," in *2016 49th Annual IEEE/ACM International Symposium on Microarchitecture (MICRO)*. IEEE, 2016, pp. 1–12.
- [2] D. Amodei, S. Ananthanarayanan, R. Anubhai, J. Bai, E. Battenberg, C. Case, J. Casper, B. Catanzaro, Q. Cheng, G. Chen *et al.*, "Deep speech 2: End-to-end speech recognition in english and mandarin," in *International conference on machine learning*, 2016, pp. 173–182.
- [3] T. Chen and C. Guestrin, "Xgboost: A scalable tree boosting system," in *Proceedings of the 22nd acm sigkdd international conference on knowledge discovery and data mining*, 2016, pp. 785–794.
- [4] T. Chen, L. Zheng, E. Yan, Z. Jiang, T. Moreau, L. Ceze, C. Guestrin, and A. Krishnamurthy, "Learning to optimize tensor programs," in *Advances in Neural Information Processing Systems*, 2018, pp. 3389–3400.
- [5] Y.-H. Chen, J. Emer, and V. Sze, "Eyeriss: A spatial architecture for energy-efficient dataflow for convolutional neural networks," *ACM SIGARCH Computer Architecture News*, vol. 44, no. 3, pp. 367–379, 2016.
- [6] Y.-H. Chen, T.-J. Yang, J. Emer, and V. Sze, "Eyeriss v2: A flexible accelerator for emerging deep neural networks on mobile devices," *IEEE Journal on Emerging and Selected Topics in Circuits and Systems*, vol. 9, no. 2, pp. 292–308, 2019.
- [7] W. J. Dally, Y. Turakhia, and S. Han, "Domain-specific hardware accelerators," *Communications of the ACM*, vol. 63, no. 7, pp. 48–57, 2020.
- [8] S. Dave, Y. Kim, S. Avancha, K. Lee, and A. Shrivastava, "Dmazerunner: Executing perfectly nested loops on dataflow accelerators," *ACM Transactions on Embedded Computing Systems (TECS)*, vol. 18, no. 5s, pp. 1–27, 2019.
- [9] R. H. Dennard, F. H. Gaensslen, V. L. Rideout, E. Bassous, and A. R. LeBlanc, "Design of ion-implanted mosfet's with very small physical dimensions," *IEEE Journal of Solid-State Circuits*, vol. 9, no. 5, pp. 256–268, 1974.
- [10] J. Fowers, K. Ovtcharov, M. Papamichael, T. Massengill, M. Liu, D. Lo, S. Alkalay, M. Haselman, L. Adams, M. Ghandi *et al.*, "A configurable cloud-scale dnn processor for real-time ai," in *2018 ACM/IEEE 45th Annual International Symposium on Computer Architecture (ISCA)*. IEEE, 2018, pp. 1–14.
- [11] M. Gao, J. Pu, X. Yang, M. Horowitz, and C. Kozyrakis, "Tetris: Scalable and efficient neural network acceleration with 3d memory," in *Proceedings of the Twenty-Second International Conference on Architectural Support for Programming Languages and Operating Systems*, 2017, pp. 751–764.
- [12] M. Gao, X. Yang, J. Pu, M. Horowitz, and C. Kozyrakis, "Tangram: Optimized coarse-grained dataflow for scalable nn accelerators," in *Proceedings of the Twenty-Fourth International Conference on Architectural Support for Programming Languages and Operating Systems*, 2019, pp. 807–820.
- [13] S. Ghodrati, B. H. Ahn, J. K. Kim, S. Kinzer, B. R. Yatham, N. Alla, H. Sharma, M. Alian, E. Ebrahimi, N. S. Kim *et al.*, "Planaria: Dynamic architecture fission for spatial multi-tenant acceleration of deep neural networks," in *2020 53rd Annual IEEE/ACM International Symposium on Microarchitecture (MICRO)*. IEEE, 2020, pp. 681–697.
- [14] K. Hegde, P.-A. Tsai, S. Huang, V. Chandra, A. Parashar, and C. W. Fletcher, "Mind mappings: enabling efficient algorithm-accelerator mapping space search," in *Proceedings of the 26th ACM International Conference on Architectural Support for Programming Languages and Operating Systems*, 2021, pp. 943–958.
- [15] N. P. Jouppi, C. Young, N. Patil, D. Patterson, G. Agrawal, R. Bajwa, S. Bates, S. Bhatia, N. Boden, A. Borchers *et al.*, "In-datacenter performance analysis of a tensor processing unit," in *Proceedings of the 44th Annual International Symposium on Computer Architecture*, 2017, pp. 1–12.
- [16] S.-C. Kao, G. Jeong, and T. Krishna, "Confucius: Autonomous hardware resource assignment for dnn accelerators using reinforcement learning," in *2020 53rd Annual IEEE/ACM International Symposium on Microarchitecture (MICRO)*. IEEE, 2020, pp. 622–636.
- [17] S.-C. Kao and T. Krishna, "Gamma: Automating the hw mapping of dnn models on accelerators via genetic algorithm," in *ICCAD*, 2020.
- [18] D. Kim, J. Kung, S. Chai, S. Yalamanchili, and S. Mukhopadhyay, "Neurocube: A programmable digital neuromorphic architecture with high-density 3d memory," *ACM SIGARCH Computer Architecture News*, vol. 44, no. 3, pp. 380–392, 2016.
- [19] T. Krishna, C.-H. O. Chen, W.-C. Kwon, and L.-S. Peh, "Smart: single-cycle multihop traversals over a shared network on chip," *IEEE micro*, vol. 34, no. 3, pp. 43–56, 2014.
- [20] H. Kwon, P. Chatarasi, M. Pellauer, A. Parashar, V. Sarkar, and T. Krishna, "Understanding reuse, performance, and hardware cost of dnn dataflow: A data-centric approach," in *Proceedings of the 52nd Annual IEEE/ACM International Symposium on Microarchitecture*, 2019, pp. 754–768.
- [21] H. Kwon and T. Krishna, "Opensmart: Single-cycle multi-hop noc generator in bsv and chisel," in *2017 IEEE International Symposium on Performance Analysis of Systems and Software (ISPASS)*. IEEE, 2017, pp. 195–204.
- [22] H. Kwon, A. Samajdar, and T. Krishna, "Maeri: Enabling flexible dataflow mapping over dnn accelerators via reconfigurable interconnects," *ACM SIGPLAN Notices*, vol. 53, no. 2, pp. 461–475, 2018.
- [23] J. Kwon, M. M. Ziegler, and L. P. Carloni, "A learning-based recommender system for autotuning design flows of industrial high-performance processors," in *2019 56th ACM/IEEE Design Automation Conference (DAC)*. IEEE, 2019, pp. 1–6.
- [24] W. Lu, G. Yan, J. Li, S. Gong, Y. Han, and X. Li, "Flexflow: A flexible dataflow accelerator architecture for convolutional neural networks," in *2017 IEEE International Symposium on High Performance Computer Architecture (HPCA)*. IEEE, 2017, pp. 553–564.
- [25] A. Mirhoseini, H. Pham, Q. V. Le, B. Steiner, R. Larsen, Y. Zhou, N. Kumar, M. Norouzi, S. Bengio, and J. Dean, "Device placement optimization with reinforcement learning," *arXiv preprint arXiv:1706.04972*, 2017.
- [26] M. Naumov, D. Mudigere, H.-J. M. Shi, J. Huang, N. Sundaraman, J. Park, X. Wang, U. Gupta, C.-J. Wu, A. G. Azzolini *et al.*, "Deep learning recommendation model for personalization and recommendation systems," *arXiv preprint arXiv:1906.00091*, 2019.
- [27] M. K. Papamichael, P. Milder, and J. C. Hoe, "Nautilus: Fast automated ip design space search using guided genetic algorithms," in *Proceedings of the 52nd Annual Design Automation Conference*, 2015, pp. 1–6.
- [28] A. Parashar, P. Raina, Y. S. Shao, Y.-H. Chen, V. A. Ying, A. Mukkara, R. Venkatesan, B. Khailany, S. W. Keckler, and J. Emer, "Timelooop: A systematic approach to dnn accelerator evaluation," in *2019 IEEE international symposium on performance analysis of systems and software (ISPASS)*. IEEE, 2019, pp. 304–315.
- [29] F. Pedregosa, G. Varoquaux, A. Gramfort, V. Michel, B. Thirion, O. Grisel, M. Blondel, P. Prettenhofer, R. Weiss, V. Dubourg, J. Vanderplas, A. Passos, D. Cournapeau, M. Brucher, M. Perrot, and E. Duchesnay, "Scikit-learn: Machine learning in Python," *Journal of Machine Learning Research*, vol. 12, pp. 2825–2830, 2011.
- [30] E. Qin, A. Samajdar, H. Kwon, V. Nadella, S. Srinivasan, D. Das, B. Kaul, and T. Krishna, "Sigma: A sparse and irregular gemm accelerator with flexible interconnects for dnn training," in *2020 IEEE International Symposium on High Performance Computer Architecture (HPCA)*, 2020.
- [31] S. Ren, K. He, R. Girshick, and J. Sun, "Faster r-cnn: Towards real-time object detection with region proposal networks," in *Advances in neural information processing systems*, 2015, pp. 91–99.
- [32] A. Samajdar, T. Garg, T. Krishna, and N. Kapre, "Scaling the cascades: Interconnect-aware fpga implementation of machine learning problems," in *2019 29th International Conference on Field Programmable Logic and Applications (FPL)*. IEEE, 2019, pp. 342–349.
- [33] A. Samajdar, J. M. Joseph, Y. Zhu, P. Whatmough, M. Mattina, and T. Krishna, "A systematic methodology for characterizing scalability of dnn accelerators using scale-sim," in *2020 IEEE International Symposium on Performance Analysis of Systems and Software (ISPASS)*, 2020.

- [34] A. Samajdar, Y. Zhu, P. Whatmough, M. Mattina, and T. Krishna, "Scale-sim: Systolic cnn accelerator simulator," *arXiv preprint arXiv:1811.02883*, 2018.
- [35] Y. S. Shao, J. Clemons, R. Venkatesan, B. Zimmer, M. Fojtik, N. Jiang, B. Keller, A. Klinefelter, N. Pinckney, P. Raina *et al.*, "Simba: Scaling deep-learning inference with multi-chip-module-based architecture," in *Proceedings of the 52nd Annual IEEE/ACM International Symposium on Microarchitecture*, 2019, pp. 14–27.
- [36] D. Silver, J. Schrittwieser, K. Simonyan, I. Antonoglou, A. Huang, A. Guez, T. Hubert, L. Baker, M. Lai, A. Bolton *et al.*, "Mastering the game of go without human knowledge," *Nature*, vol. 550, no. 7676, pp. 354–359, 2017.
- [37] C. Zhang, P. Li, G. Sun, Y. Guan, B. Xiao, and J. Cong, "Optimizing fpga-based accelerator design for deep convolutional neural networks," in *Proceedings of the 2015 ACM/SIGDA International Symposium on Field-Programmable Gate Arrays*, 2015, pp. 161–170.
- [38] Z. Zhao, H. Kwon, S. Kuhar, W. Sheng, Z. Mao, and T. Krishna, "mrna: Enabling efficient mapping space exploration for a reconfiguration neural accelerator," in *2019 IEEE International Symposium on Performance Analysis of Systems and Software (ISPASS)*. IEEE, 2019, pp. 282–292.